LETTER Communicated by Richard Krauzlis

Vergence Dynamics Predict Fixation Disparity

Saumil S. Patel
College of Optometry and Department of Electrical and Computer Engineering, University of Houston, Houston, TX 77204, U.S.A.

Bai-Chuan Jiang
College of Optometry, Nova Southeastern University, Ft. Lauderdale, FL 33328, U.S.A.

Haluk Ogmen
Department of Electrical and Computer Engineering, University of Houston, Houston, TX 77204, U.S.A.

The neural origin of the steady-state vergence eye movement error, called binocular fixation disparity, is not well understood. Further, there has been no study that quantitatively relates the dynamics of the vergence system to its steady-state behavior, a critical test for the understanding of any oculomotor system. We investigate whether fixation disparity can be related to the dynamics of opponent convergence and divergence neural pathways. Using binocular eye movement recordings, we first show that opponent vergence pathways exhibit asymmetric angle-dependent gains. We then present a neural model that combines physiological properties of disparity-tuned cells and vergence premotor cells with the asymmetric gain properties of the opponent pathways. Quantitative comparison of the model predictions with our experimental data suggests that fixation disparity can arise when *asymmetric* opponent vergence pathways are driven by a distributed disparity code.

1 Introduction

Central to the understanding of human behavior is the understanding of neural sensorimotor systems that produce the behavior. The eye movement system is one of the best understood sensorimotor systems in the brain. Binocular gaze shifts in space are achieved by simultaneous operation of two classes of eye movement subsystems: conjugate and disjunctive. The disjunctive system, which is also called the vergence system, maintains optical alignment of both eyes when viewing a target binocularly. For a gaze shift between targets at different depths, it responds in a manner that reduces the resulting binocular disparity, thus maintaining single vision. The sensorimotor architecture of the vergence system is poorly understood. Experience from conjugate eye movement system studies suggests that sig-

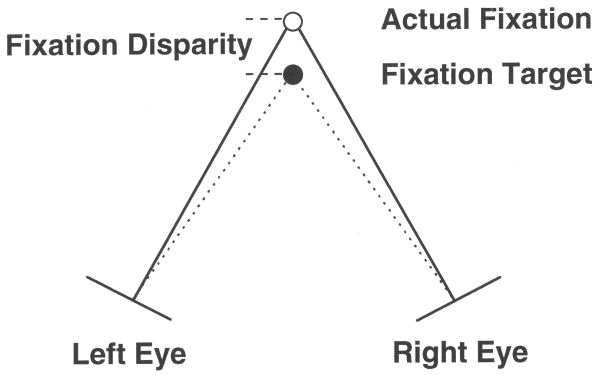

Figure 1: An illustration of fixation disparity. The eyes are fixating on a point (unfilled circle) that is less convergent than the target position (filled circle). The difference between the target position and the actual fixation point of the eyes represents the fixation disparity.

nificant understanding of mechanisms of eye movements is possible when physiological and behavioral aspects of the system are incorporated into an analytical model that provides accurate predictions of the static and dynamic oculomotor responses under a variety of stimulus conditions (Robinson, 1981). However, for the vergence system, relatively few attempts (see Keller, 1981; Mays, 1984; Mays, Porter, Gamlin, & Tello, 1986; Gamlin, Gnadt, & Mays, 1989; Gamlin & Mays, 1992) have been made to combine physiological and behavioral evidence analytically. Even fewer attempts have been made to relate steady-state properties to the dynamic properties of the system. In this article, we seek to relate fixation disparity, a static vergence error, to the dynamics of the vergence system using a model that combines behavioral properties of the vergence system with the neurophysiological characteristics of disparity-tuned sensory and premotor vergence cells.

The difference between the position of a fixation target and the point actually fixated by the eyes is called fixation disparity (see Figure 1). The basis of this ocular misalignment, which has been observed for a century (see Ogle, Martens & Dyer, 1967), is largely unknown. As a consequence of fixation disparity, the fixation target is imaged away from the central parts of the fovea in either one or both eyes, therefore degrading the quality of the images available for fine stereopsis. Excessive fixation disparity has been associated with some types of binocular dysfunction, though its use as a general predictor of binocular stress and dysfunction has been difficult and at times unsuccessful (see Ogle et al., 1967). One of the main reasons for the failure of fixation disparity to predict binocular dysfunction lies in the fact that the neural origin of this error has not been well understood. Existing

control-type models of the vergence system (Ogle et al., 1967; Schor 1979a, 1979b; Hung & Semmlow, 1980; Schor, Robertson, & Wesson, 1986; Saladin, 1986), suggest that fixation disparity results from the leakiness of position integrators (Schor 1979a, 1979b; Hung & Semmlow, 1980; Schor et al., 1986; Saladin, 1986). However, most reports in the literature favor a non-leaky integration in the vergence system (Rashbass & Westheimer, 1961; Zuber & Stark, 1968; Semmlow, Hung, Horng, & Ciuffreda, 1994), although there has been an isolated report to the contrary (Pobuda & Erkelens, 1993). Despite the evidence against leaky integration, these models required the leakiness to account for the decay of vergence angle in the absence of binocular stimulus (Krishnan & Stark, 1977). However, as suggested by a recent neural network model (Patel, Ogmen, White, & Jiang, 1997), a nonlinear active turn-off circuit in conjunction with a nonleaky integrator (nonleaky with respect to the time-scale of the dynamics) would achieve the same behavioral function. Moreover, this neural network model can explain a much wider range of vergence dynamic data compared to alternative control-type models (Patel et al., 1997). Unlike control-type models, this model can also correlate behavioral responses to underlying neurophysiological components of the vergence system. On the other hand, nonleaky integration in general implies zero position error, that is, zero fixation disparity. As suggested by a previous analysis (Patel et al., 1997), a model with nonleaky integration coupled with an asymmetry between the dynamics of convergence and divergence pathways can offer an alternative explanation for fixation disparity. In this article, we present experimental evidence supporting this hypothesis.

2 Model Description

2.1 Dynamic Model. A neural network model of horizontal disparity vergence dynamics (Patel et al., 1997) is shown in Figure 2a. Only those portions of the model that play an active role during binocular fixation are shown. Prior to a vergence movement, the binocular target activates a subset of disparity encoders that signal the presence of a nonzero initial binocular disparity. Two types of disparity encoders are employed in the model: convergence encoders and divergence encoders. In the model, we have used the word *encoder* instead of *disparity-tuned cell* because, as mentioned in our earlier work (Patel, Ogmen, & Jiang, 1996; Patel et al., 1997), it is not clear whether the same cells that may be responsible for the perception of depth (Barlow, Blakemore, & Pettigrew, 1967; Poggio, Gonzalez and Krause, 1988; Roy, Komatsu, & Wurtz, 1992) are also responsible for the vergence movements. Recent evidence suggests that the disparity cells responsible for vergence movements might not be directly responsible for perception of depth (Cumming & Parker, 1997; Masson, Busettini, & Miles, 1997). Functionally, convergence and divergence encoders are equivalent to near-tuned excitatory and far-tuned excitatory disparity cells, respectively.

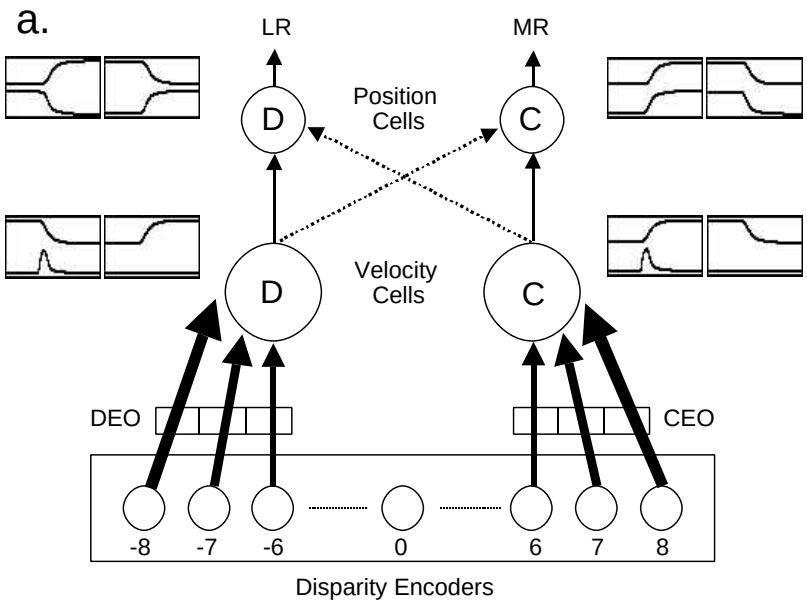

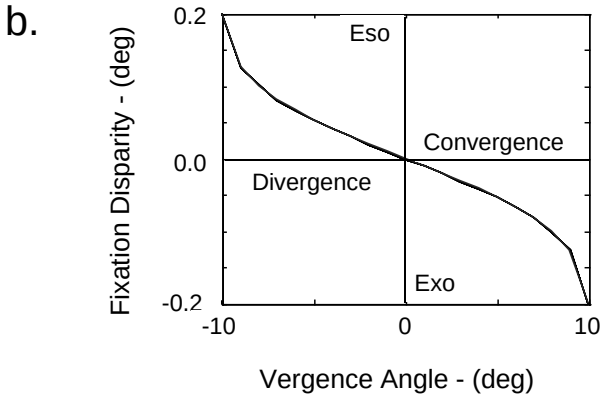

The disparity encoders are topographically ordered in a horizontal direction such that the central encoder signals zero disparity and encoders positioned on either side of the zero disparity encoder signal disparity proportional to their Euclidean distance from zero disparity. The encoders to the right (left) of the zero disparity encoder signal crossed (uncrossed) disparity. To understand the operation of the model, consider the case where the eyes are presented with a target whose images on the two retinas induce a disparity.

This retinal disparity will generate an activation pattern across the population of disparity encoders. For simplicity, we will first consider the case where the activation pattern consists of the activity of a *single* encoder, that is, a spatially localized disparity code. A vergence velocity signal will be formed based on the sign of the disparity represented by this encoder; a crossed disparity activates the convergence velocity cell, and an uncrossed disparity activates the divergence velocity cell. The strength of the innervation of the velocity cell is proportional to the magnitude of the disparity. The velocity signal drives a pair of vergence position cells in a push-pull manner. The position cells exhibit nonlinear shunting type membrane dynamics (Grossberg, 1988). The convergence position cell projects to medial rectus motoneurons, and the divergence position cell projects to lateral rectus motoneurons of both eyes. The eye plant is a first-order linear system (Robinson, 1981; Krishnan & Stark, 1983). The initial disparity therefore results in a movement of both eyes in opposite directions—that is, a vergence

Figure 2: *Facing page*. (a) Sensorimotor transformation and push-pull integration in the neural network model of disparity vergence system. Only the portions of the model that play a role during binocular fixation are shown. All solid (dotted) lines represent excitatory (inhibitory) connections. The cells in the convergence pathways are labeled *C*, and those in divergence pathways are labeled D. The graded connectivity between the disparity encoder cells and the velocity cells represents the sensorimotor transformation and is shown by variable-thickness lines on both sides of the figure. Thicker lines depict larger synaptic weights. The convergence (divergence) encoders send excitatory projections to convergence (divergence) velocity cells. *CEO* (*DEO*) is a vector of the outputs of the convergence (divergence) encoders. The numbers under the disparity encoders represent their position in the map of disparity encoders. The velocity cells project in a push-pull manner (e.g., convergence velocity cell sends excitatory projections to convergence position cell, and divergence velocity cell sends inhibitory projections to convergence position cell) to position cells, which in turn project to medial and lateral rectus sections (*LR*, *MR*) of the motoneurons / plant system for each eye. The firing profiles of the vergence velocity cells and the vergence position cells in the model are shown in rectangular boxes besides the corresponding cells. The top trace within each box is the simulated vergence step movement of 2 degrees for which the corresponding firing profiles are obtained. The bottom trace is the firing rate of the corresponding cell. Upward deflection in the vergence traces indicate increased convergence and downward deflection indicates increased divergence. The firing profiles of model neurons are very similar to those of actual cells found in primate midbrain (Mays, 1984, Mays et al., 1986). (b) Steady-state vergence error exhibited by the neural network model shown in *a*. This error characteristic is obtained by a parameter set that is equal for cells in both convergence and divergence pathways. A rectangular binary disparity code is used (see main text). (Adapted Patel et al., 1997)

movement that reduces the disparity of the target. The reduced disparity will activate the disparity encoder representing this new value of the target disparity. This cyclic process will continue until the disparity is reduced to zero. In other words, at steady state, only the encoder signaling *zero* disparity will be active. In summary, if disparity is represented by the activity of a *single* disparity encoder, the model will reach steady-state where fixation disparity is zero.

To facilitate the understanding of the derivation of the static model from the dynamic model, let us first describe the dynamic model shown in Figure 2a in simple mathematical terms. The vergence output (*VO*), defined as the difference between the angle of horizontal rotation of the two eyes, can be simply written as:

$$VO(t) = F(CEO, DEO, LR, MR, t) \tag{2.1}$$

where F is some nonlinear function that represents the entire vergence feedback system, *CEO* (*DEO*) is a *vector* of the outputs of the convergence (divergence) encoders, *LR* (*MR*) is the output to the motoneurons innervating lateral (medial) rectus muscles of both eyes, and t is time.

Let us define the two subtypes of mutually exclusive vergence outputs:

$$VOC(t) = FC(CEO, LR, MR, t) \tag{2.2}$$

$$VOD(t) = FD(DEO, LR, MR, t) \tag{2.3}$$

where *VOC* (or convergence) is the vergence position when *DEO* is zero, *VOD* (or divergence) is the vergence position when *CEO* is zero and, *FC* and *FD* are some nonlinear functions. In otherwords, convergence movement is induced by activation of the sensorimotor pathways innervated by the convergence encoders, and divergence movement is induced by activation of the sensorimotor pathways innervated by the divergence encoders. Notice that due to the push-pull integration of the vergence velocity signals, these two functionally separate movements share common physical pathways.

Because the sensory and motor components are arranged in a feedforward cascade manner, we assume that for each type of movement, the sensory and motor components are functionally separable then,

$$VOC(t) = FCS(CEO, t) * FCM(CV, LR, MR, t) \tag{2.4}$$

$$VOD(t) = FDS(DEO, t) * FDM(DV, LR, MR, t) \tag{2.5}$$

where *FCS* (*FDS*) and *FCM* (*FDM*) are sensory and motor functions for convergence (divergence) and *CV* (*DV*) is the output of the convergence (divergence) sensory component.

When convergence and divergence movements are induced simultaneously by a distributed disparity code, an equilibrium can only be reached

if both movements are equal in magnitude. In this case of simultaneous activation, if we define the vergence imbalance as

$$VI(t) = VOC(t) - VOD(t), \tag{2.6}$$

then at equilibrium (steady state) we have

$$VI(\text{infinity}) = 0. \tag{2.7}$$

2.2 Fixation Disparity Simulated from the Dynamic Model. Previous studies on disparity-sensitive neurons have generally found cells that have broad as opposed to binary (on-off) tuning functions (Barlow et al., 1967; Roy, Komatsu, & Wurtz, 1992; Gonzalez, Relova, Perez, Acuna, & Alonso, 1993; Wagner & Frost, 1993). This implies that a given target disparity activates more than one disparity encoder, i.e. a spatially distributed code. Further, in humans, it has been proposed that vergence control is based on a *population* code formed by a pool of disparity tuned cells (Mallot, Roll, & Arndt, 1996; Patel et al., 1997). The optics of the eye cause the image of a visual point to spread on the retina (see Charman, 1991). This, coupled with cross-correlation of images from the two eyes (Stevenson, Cormack, & Schor 1994), suggests that even small targets (∼2–4 arc-min) would generate a spatially distributed disparity code. As a consequence of the broad tuning property of disparity cells, binocular disparity due to a target would be coded in a distributed manner. In our model, as a result of the disparity spread, both convergence and divergence disparity encoders will be excited at steady state. This simultaneous activation of convergence and divergence disparity encoders will result in simultaneous activation of convergence and divergence velocity cells. An equilibrium will be achieved when the convergence and divergence motor activity due to simultaneous activation of convergence and divergence velocity cells balances each other. The displacement of the centroid of the disparity spread relative to the zero disparity encoder is then the fixation disparity. If the disparity code is perfectly symmetric and the convergence and divergence pathways are also perfectly symmetric for all vergence angles, then the fixation disparity is zero for all those vergence angles. On the other hand, for a symmetric disparity code, any asymmetry in convergence and divergence pathways (sensory or motor or both components) would result in a nonzero fixation disparity. As shown in Figure 2b, the neural network model, when simulated by a *rectangular disparity code*, exhibits a nonlinear steady-state error function with respect to vergence angle. A *rectangular disparity code* can be formed when a set of cells within a topographic map of cells fires equally in response to a given input. Normally, in a distributed sensory code, the firing pattern as a function of cell position in the topographic map would be symmetric and decreasing (e.g., gaussian) around the cell firing maximally. However, the assumption of a rectangular code greatly simplifies the

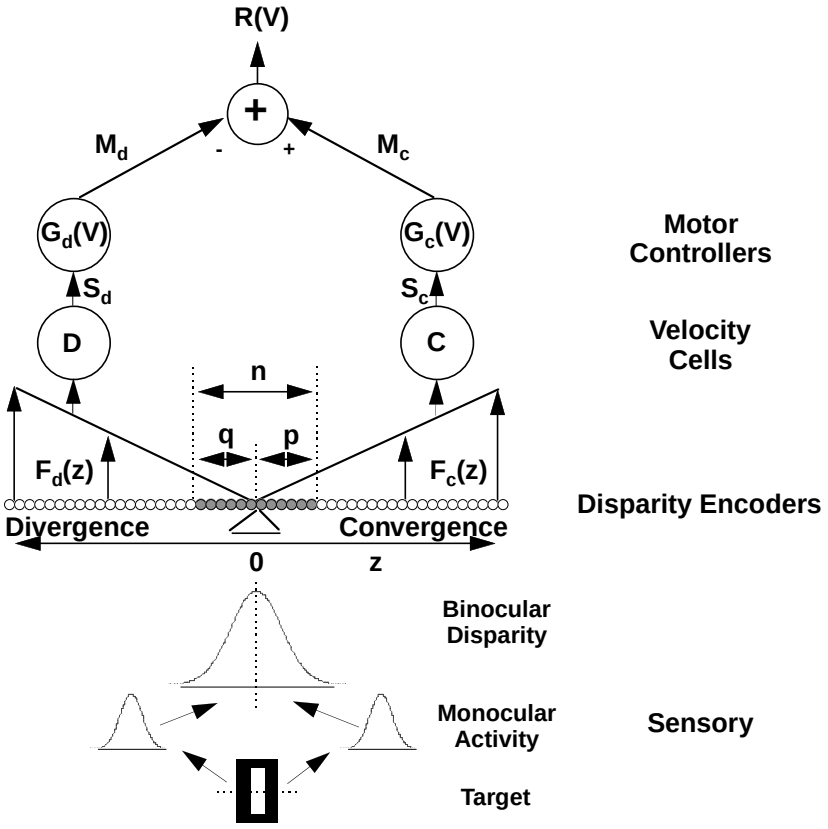

steady-state analysis without losing generality. The steady-state vergence error function shown in Figure 2b comes as a result of asymmetry in dynamics generated by the nonlinear push-pull integration architecture. We also tested a gaussian and a triangular disparity code and found that the qualitative nature of the steady-state vergence error function was similar to that shown in Figure 2b.

2.3 Static Model. In order to write a simple analytical formula for fixation disparity, a simplified form of the neural network model is derived (see Figure 3). The original neural network model and its simplified version will be hereafter called dynamic vergence model and static vergence model, respectively. We now consider the static model shown in Figure 3. In the nervous system and the dynamic model, disparity is encoded by the activities of a discrete set of neurons. To simplify the analysis, in the static model we use a continuous variable (z) to represent disparity. This simplification is justified if one considers that the set of disparity encoders contains

a large number of neurons. A consequence of this simplification is that the discrete synaptic weights between the disparity encoders and velocity cells are replaced by continuous functions ($F_c(z)$ and $F_d(z)$) in the static model. Because we are interested in the origin of fixation disparity, our analysis is restricted to the vergence system and assumes that the lens accommodation system is functionally in an open-loop condition.

We use a binary rectangular disparity code to illustrate the principles of our model. The aggregate sensory output from crossed and uncrossed sides is determined by the spatial extent n and location of the disparity spread (p and q) generated by the target (see Figure 3). Note that p and q represent the disparity spread relative to an absolute disparity and should not be confused with absolute disparity represented by z. In ideal steady-state condition, the absolute disparity around which they are defined is 0. The disparity encoder for disparity z projects to velocity cell with a synaptic weight represented by $F(z)$. If this cell is active, its synaptic effect will be given by $F(z)$, and if it is inactive, its postsynaptic effect will be zero. Because velocity cells summate their inputs, the output of divergence ($S_d(z)$) and convergence ($S_c(z)$) velocity cells can be written as

$$S_d = \int_0^{-q} F_d(z)dz \text{ and } S_c = \int_0^{p} F_c(z)dz, \tag{2.8}$$

where z is the disparity, F_d and F_c are sensorimotor transformation functions for divergence and convergence pathways, respectively, and integration (as

Figure 3: *Facing page*. Static vergence model. The lower part of the figure shows an example of a disparity code formed by cross-correlation of monocular activity that is induced by a white line target (consider one dimension as indicated by a horizontal dotted line). The horizontal axis represents a mapping of visual space onto a line of neurons. The fulcrum represents the zero disparity point. The horizontal line extending in the z direction from the fulcrum represents a continuous array of horizontal disparity encoders. The negative (positive) z-axis represents divergence (convergence) encoders. The disparity encoders activated by the disparity spread of the target are shaded in gray. The points p and q represent the end points of the disparity spread, and n is the total extent of the spread. The sensory contribution of each active divergence and convergence disparity encoder is represented by $F_d(z)$ and $F_c(z)$, respectively, where z denotes disparity (the position in the array of horizontal disparity encoders). S_c and S_d are the output of vergence velocity cells (C and D). The gains of divergence and convergence motor controllers are represented by $G_d(V)$ and $G_c(V)$. The steady-state vergence angle is denoted by V, and the vergence imbalance for that angle, R, is defined as the difference between the divergence and convergence motor outputs M_d and M_c, respectively, and is zero at steady state The eye plant is not shown but is assumed to be a first-order linear system, and therefore at steady state, its contribution is just a constant gain factor.

opposed to summation) is used to take into account the continuous nature of z. S_c and S_d correspond to *CV* and *DV* in equations 2.4 and 2.5. The functions that relate S_c and S_d to z correspond to *FCS* and *FDS* in equations 2.4 and 2.5. A sensorimotor transformation function transforms a given sensory variable to a motor variable. In our case, the sensory variable is target disparity and motor variable is a correlate of vergence velocity.

Although the vergence position cells in the dynamic model integrate their inputs nonlinearly over the entire range of vergence movements, for a small vergence movement (small-signal linearity), the temporal integration of the output of the velocity cells by the vergence position cells can be considered linear. Thus, at steady state only a gain that depends on the initial vergence angle (the large signal) relates the output of the velocity cells to the output of the position cells. Further, the eye plant is also linear; thus, at steady state, it is the final gain stage in the vergence pathway. Therefore, the experimentally measured linear relationship between target disparity and the velocity of the vergence movement for at least the ± 2 degree disparity range (Rashbass & Westheimer, 1961) implies a linear relationship between target disparity and the output of the velocity cells in our model (see the appendix for a formal derivation). We therefore choose the functions F_d and F_c to be linear functions of z,

$$F_d(z) = K_d z \text{ and } F_c(z) = K_c z, \tag{2.9}$$

where K_d and K_c are defined as divergence and convergence sensory gains, respectively. In the dynamic model, these gains are represented by the weights of the crossed and uncrossed disparity signals as they feed into the corresponding velocity cells. Therefore, in the dynamic vergence model, the sensorimotor transformation is performed by the vergence velocity cells.

Substituting equation 2.9 in equation 2.8, we obtain

$$S_d = \frac{K_d q^2}{2} \text{ and } S_c = \frac{K_c p^2}{2}. \tag{2.10}$$

The steady-state outputs M_d and M_c of divergence and convergence motor controllers can then be calculated as

$$M_d = S_d G_d(V) = \frac{K_d q^2 G_d(V)}{2} \text{ and } M_c = S_c G_c(V) = \frac{K_c p^2 G_c(V)}{2}, \tag{2.11}$$

where V is the steady-state vergence angle. $G_c(V)$ and $G_d(V)$ are defined as angle-dependent convergence and divergence motor gains respectively, and, correspond to *FCM* and *FDM* in equations 2.4 and 2.5. M_c and M_d correspond to *VOC* and *VOD* in equations 2.2 and 2.3 when the pathway downstream of the vergence position cells is assumed to be linear. Although the relationship of the steady-state output of the motor controllers is quadratic

in the parameters of the disparity spread (p and q), the relationship between disparity z and the velocity of small vergence movement (under most dynamic conditions) remains linear. As shown previously (Patel et al., 1997), the dynamic vergence model exhibits angle-dependent variable gains during convergence and divergence movements. The exact nature of the variable gains as a function of angle primarily depends on the parameters defining the membrane characteristics of the vergence position cells in the dynamic model.

As indicated in Figure 3, the vergence imbalance $R(V)$ (same as VI in equation 2.6) is calculated as

$$R(V) = M_c - M_d = \frac{1}{2}[K_c p^2 G_c(V) - K_d q^2 G_d(V)]. \tag{2.12}$$

The fixation disparity $E(V)$ at a given angle V, specifically for a binary disparity code, is

$$E(V) = p - q. \tag{2.13}$$

At steady state, we have $R(V) = 0$ (same as equation 2.7) and for a rectangular binary disparity code $p+q = n$; hence, we can rewrite equations 2.12 and 2.13 in variables p and n. By eliminating p from the rewritten equations 2.12 and 2.13

$$E(V) = n\left(\frac{1-\gamma(V)}{1+\gamma(V)}\right), \tag{2.14}$$

where

$$\gamma(V) = \sqrt{\frac{K_c G_c(V)}{K_d G_d(V)}}. \tag{2.15}$$

If p and q are equal at equilibrium, then the fixation disparity is zero. If q is larger (smaller) than p, the eyes are overconverged (underconverged).

To illustrate how $K_c G_c(V)$ and $K_d G_d(V)$ can be determined experimentally, consider a time instant t during an open-loop or disparity clamped convergence movement. Let the average target disparity be denoted by d_s. Let the disparity spread be rectangular with a symmetrical spread of $n/2$ on both sides of d_s. Because the disparity input is fixed or clamped in time, the corresponding fixed or steady-state output of the convergence velocity cell would be $nK_c d_s$ (by using $S_c = \int_{d_s-\frac{n}{2}}^{d_s+\frac{n}{2}} K_c z dz$).

Because the position cells are nonleaky integrators and can be considered linear for a small range of vergence angles, the vergence angle, which is the output of the convergence motor controller, would be $nK_c d_s G_c(V)t$ (by using $M_c = \int_0^t nK_c d_s G_c(V)dt$; assume initial convergence is zero). Let us define the product $K_c G_c(V)$, which linearly relates the output convergence angle to the

input disparity as the sensory motor gain for the convergence pathway. The velocity of the convergence movement would therefore be $nK_cG_c(V)d_s$. Because the relationship between the magnitude of d_s and the experimentally measured velocity of the corresponding open-loop convergence movement is linear for small movements, the slope of this relationship can be used as an approximation for $\Psi K_cG_c(V)$ where Ψ is a constant that includes the gain of the pathway downstream of the vergence position cells. If we assume that Ψ is similar for convergence and divergence movements, then the ratio of the slopes of the relationship between d_s and the velocity of the open-loop vergence movement for convergence and divergence movements can be used to approximate the ratio of $K_cG_c(V)$ to $K_dG_d(V)$, respectively. For the purpose of forming the ratio of open-loop convergence to divergence velocity, the open loop vergence velocity measurements can further be replaced by peak vergence velocity measurements (Semmlow et al., 1994; Hung, Zhu, & Ciuffreda, 1997).

In summary, quantitative analysis of the static vergence model therefore suggests a linear relationship between fixation disparity, $E(V)$ and a function, $\lambda(V)$, of the ratio of convergence and divergence sensory motor gains where

$$\lambda(V) = \frac{1-\gamma(V)}{1+\gamma(V)}. \tag{2.16}$$

Hence, if fixation disparity is a result of asymmetry between convergence and divergence dynamics, then a strong correlation should exist between $E(V)$ and $\lambda(V)$. This prediction was tested experimentally by a simple staircase-pulse paradigm (see Figure 4a).

3 Methods

Five subjects (*LFH*, *JCK*, *VTA*, *NYN*, and *HNG*) participated in this study voluntarily. All the subjects were emmetropic. All had at least 20/20 visual

Figure 4: *Facing page.* (a) The stimulus paradigm used in our experiments. Upward deflection in the stimulus trace represents increased convergence demand. The dotted horizontal lines represent the three pedestal demands used in the experiments. (b) A typical vergence recording in our experiments. The right and left eye position signals are shown in the top two traces (RE, LE; sampling rate 60 Hz). The unfiltered vergence signal (RV) is obtained by subtracting RE from LE. The filtered vergence signal (FV) is obtained by digitally low-pass filtering RV with a cut-off frequency of 5 Hz. The vergence velocity signal (VV) is computed by differentiating FV. The bottom trace shows the stimulus with each step in the paradigm corresponding to a 2 degree symmetric vergence demand (except a 1 degree first step during staircase). Upward deflection indicates increased convergence demand.

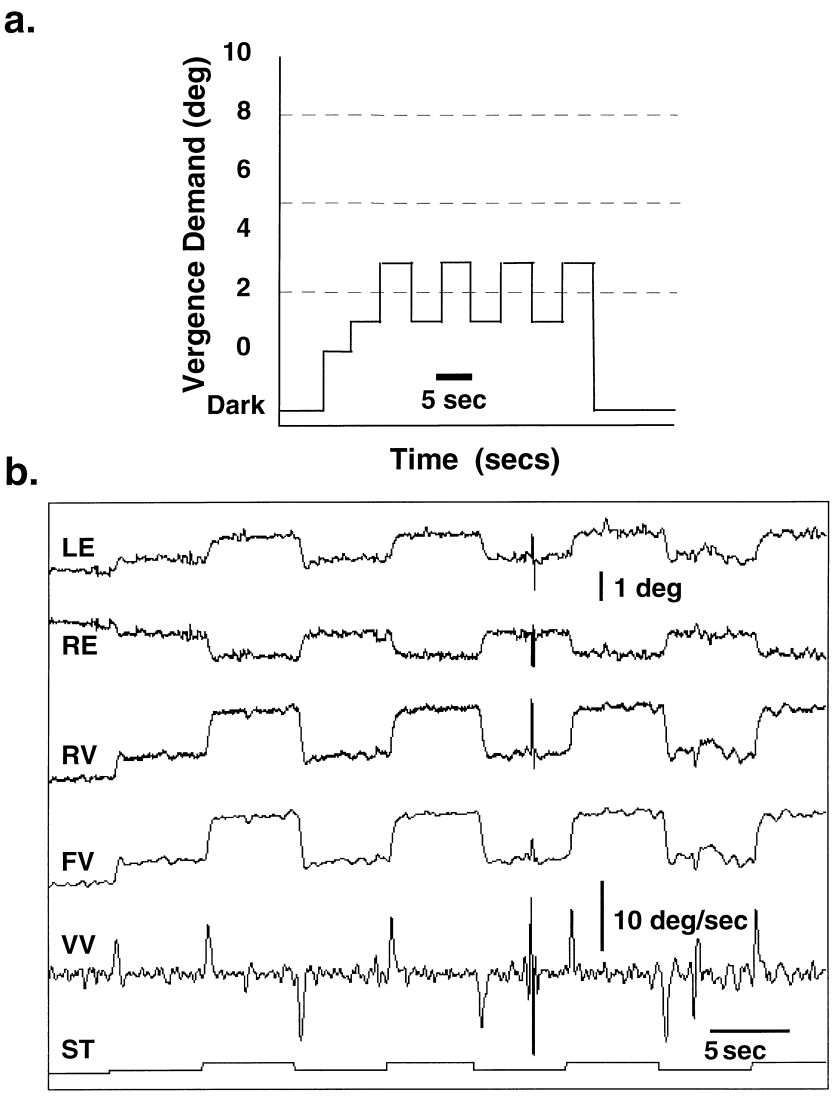

acuity with normal binocular vision. Horizontal eye movements of both eyes were measured with a pair of dual Purkinje-image eye trackers (Crane & Steele, 1978). In a dark room, using the Badal optical systems of the stabilizing attachments to the eye trackers, the subject viewed a pair of bright vertical lines (9 degrees in length and 0.35 degree in width; 0.56 candelas per square meter), one presented to each eye on separate monitors with dark background via mirrors positioned in front of the eye trackers. Each

monitor was placed at a distance of 1 m from the exit pupil of the corresponding eye tracker. During target viewing, the subject rested his or her chin on a chin rest, and head movements were restricted using a forehead support. A Macintosh II computer controlled the stimulus display and collected data at a sampling rate of 60 Hz per channel, using a 12-bit A/D converter. Two D/A channels were used to map the current stimulus position on each screen. These mapped signals were also recorded along with the eye movement signals. All data were analyzed using the data analysis package AcqKnowledge (BIOPAC Systems Inc.). Instead of pinhole viewing, we used a low-luminance, low-spatial-frequency target that greatly reduces the accommodative gain (Campbell, 1954; Johnson, 1976). It can be shown that as far as the relationship between fixation disparity and vergence demand is concerned, a reduction in accommodation gain of a log unit is effectively the same as opening the accommodative control loop (Schor, 1992).

One at a time, the target on each monitor was initially aligned to force the corresponding eye to look straight ahead. This alignment was achieved by placing a rectangular grid close to the subject's viewing eye. The target was adjusted (vertically and horizontally using keyboard) until the subject aligned the center of the target with the center of the grid. After this alignment procedure was completed for both eyes, the grid was removed from the optical path, and the subject was asked to fuse the targets. In case the subject had vertical phoria, an additional vertical adjustment was performed on one of the two targets until fusion was established. The initial monocular alignment that resulted in binocular viewing at 0 degree (parallel eyes) was fixed during all subsequent sessions. The distance of the display monitors was moved from 1 m (physical) to 4 m (optical) by placing a convex lenses of 0.75D in the optical path of each eye. Due to the haploscopic viewing in our experiments, the vergence demand can be manipulated independent of the constant accommodation demand.

Calibration of the eye tracker, conducted in each session of the experiments, was accomplished by presenting a monocular target at different fixation directions for each eye and recording the related eye movement. Based on the eye tracker calibration, the signal recorded from each eye tracker was converted to eye position. The vergence response was then computed by subtracting the two eye position signals (see Figure 4b). Since vergence responses are attenuated by 40 dB around 4 Hz (Zuber & Stark, 1968), the vergence signal was digitally low-pass-filtered at 5 Hz (see Figure 4b).

In the experiment, vergence demand was toggled between convergence and divergence around a pedestal (or average) demand using three 2 degree peak-to-peak pulses of 5 seconds (see Figure 4a). Three pulses were used for purposes of averaging to improve the signal-to-noise ratio of the vergence signal. The duration of 5 sec was used to avoid adaptive effects (Sethi, 1986). Three pedestal convergence demands were used in random order: 2, 5 and 8 from a 0 degree demand, which represents a parallel angle for the two eyes. A staircase paradigm comprising multiple 2 degree steps

was used to achieve each pedestal demand. For 2 and 8 degree pedestal demand, the first step was 1 degree instead of 2 degrees, as shown in the example in Figure 4a. The duration of each step in the staircase was 5 seconds. The vergence velocity was computed by differentiating the filtered vergence signal (see Figure 4b). Positive (negative) velocity was assigned to convergence (divergence) movement. The fixation disparities at various demands were obtained from the staircase response generated during the stimulation of 8 degree pedestal demand. The fixation disparity was computed as the difference between the demand and the average vergence angle during the last 2 seconds of the step. Positive (negative) fixation disparity was assigned to underconvergence (overconvergence). The fixation disparity at pedestal demand of 2 degrees was computed by averaging the disparities at demands of 1 and 3 degrees. Similarly averaging of fixation disparities at 7 and 9 degrees pedestal demands was used to obtain the fixation disparity at pedestal demand of 8 degrees. About 10 minutes of rest was introduced between tests at different demands. Because many researchers have shown that saccades facilitate vergence movements (Enright, 1986; Zee, Fitzgibbon, & Optican, 1992; Wick & Bedell, 1992), care was taken to separate and analyze only pure-vergence movements. Unfiltered responses for which a saccade (less than 10 degrees per second or amplitude more than 0.3 degree) occurred in either eye between the onset of stimulation and 33 msec (two samples) after peak vergence velocity occurred were rejected from further analysis. Each subject was tested twice, thus providing a maximum of six pulses per pedestal demand for subsequent data analysis.

4 Results and Discussion

4.1 Dynamic Asymmetry in the Vergence System. We show the existence of dynamic asymmetry, which is characterized by a pedestal demand-dependent difference in convergence and divergence velocities. Figure 5 shows typical vergence eye movement recordings for one subject (*LFH*) at pedestal demands of 2, 5, and 8 degrees. The asymmetry in peak convergence and divergence velocities increases as pedestal demand increases. All subjects showed this increase in asymmetry with increase in pedestal demand; however, the magnitude of differences between convergence and divergence peak velocities was different. The differences between occurrence times of peak convergence and divergence velocities were nonsystematic with respect to the pedestal demand. To analyze the dynamic asymmetry quantitatively, repeated measures analysis of variance (ANOVA) was performed on the peak convergence and divergence velocities and their occurrence times.

The average convergence and divergence peak velocities for all subjects are shown in Figure 6a. A three-way repeated measures ANOVA of the data in Figure 6a indicates that an increase in pedestal demand results in a significant increase in the difference between peak convergence and

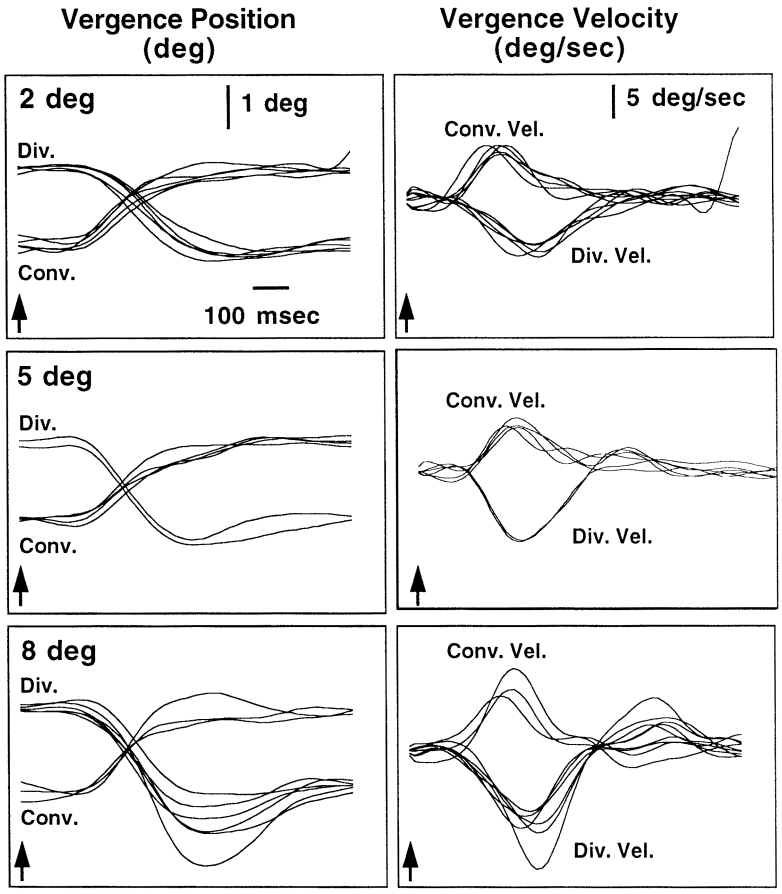

Figure 5: Vergence eye movement data from subject LFH. The left column shows vergence position traces, and the right column shows the corresponding computed vergence velocity traces. The stimulus is a 2 degree vergence step on a pedestal demand. The corresponding pedestal demand is indicated in each box containing position traces. Upward (downward) deviation in position traces indicates increased convergence (divergence). Upward (downward) deviation in velocity traces indicates positive (negative) vergence velocity. The arrows indicate the onset of the convergence or divergence step stimulus. The position, velocity, and timescales are the same for all panels. The position and velocity traces are aligned to obtain the overlap shown in the figure.

divergence velocities ($F[1, 8] = 1.1$, $p = .28$ at 2 degrees; $F[1, 8] = 38.8$, $p = .004$ at 5 degrees; $F[1, 8] = 106.9$, $p = .0005$ at 8 degrees). Furthermore, ANOVA also indicates a strong dependence of peak divergence velocity on pedestal vergence demand ($F[1, 8] = 22$, $p = .01$ between 2 and 5 degrees; $F[1, 8] = 47.1$, $p = .001$ between 2 and 8 degrees; $F[1, 8] = 17.6$, $p = .02$ between 5 and 8 degrees) but little effect of pedestal demand on peak convergence velocity ($F[1, 8] = .23$, $p = .51$ between 2 and 5 degrees; $F[1, 8] = .15$, $p = .56$ between 2 and 8 degrees; $F[1, 8] = .008$, $p = .8$ between 5 and 8 degrees). These results suggest some form of motor nonlinearity in the vergence system. Similar dependence of prior vergence angle on short-latency vergence movements induced by radial optic flow has been recently reported (Yang, Fitzgibbon, & Miles, 1998). Their data also indicate that the effect of prior vergence angle on convergence is different from that on divergence. These results suggest that vergence velocity depends on its prior angle and may partly explain why comparisons between convergence and divergence peak velocities have varied idiosyncratically between past studies (Zuber & Stark, 1968; Krishnan & Stark, 1977; Schor et al., 1986; Erkelens, Steinman, & Collewijn, 1989; Hung et al., 1997; Zee et al., 1992).

4.2 Is Asymmetry in Vergence Dynamics Due to Fixation Disparity? One might expect an effect of pedestal demand on vergence velocity due to the presence of fixation disparity. The average fixation disparity at various angles for all subjects is shown in Figure 6b. At the pedestal demands tested in our experiment, all the subjects exhibited an increase in underconvergence with an increase in pedestal demand. Because of fixation disparity, a symmetrical convergence-divergence pulse demand would stimulate the vergence system asymmetrically (see Figure 7a inset). However, a fixation disparity should affect both the convergence and divergence peak velocities. In contrast to this expectation, the data in Figure 6a clearly show that only divergence velocity is affected by the pedestal demand. To investigate the possibility further, the stimulus pulses, which were ± 1 degree around all pedestal demands (i.e., 2 degree step), were corrected for each subject based on the corresponding fixation disparities. As an example of correction, for a 2 degree pedestal demand, assume that the fixation disparity represents a 0.5 degree of underconvergence. An additional 1 degree convergence demand would then create an instantaneous convergence disparity step of 1.5 degree (corrected convergence step) and, a 1 degree divergence demand would create an instantaneous divergence disparity of 0.5 degree (corrected divergence step). In our experiments, the corrected convergence (divergence) step size was computed by adding (subtracting) the fixation disparity at the lower (upper) amplitude of the pulse demand. As shown in Figure 7a, the magnitude of the corrected stimulating step for convergence (divergence) increases (decreases) with an increase in pedestal demand. The corresponding changes in vergence velocity (see Figure 6a)

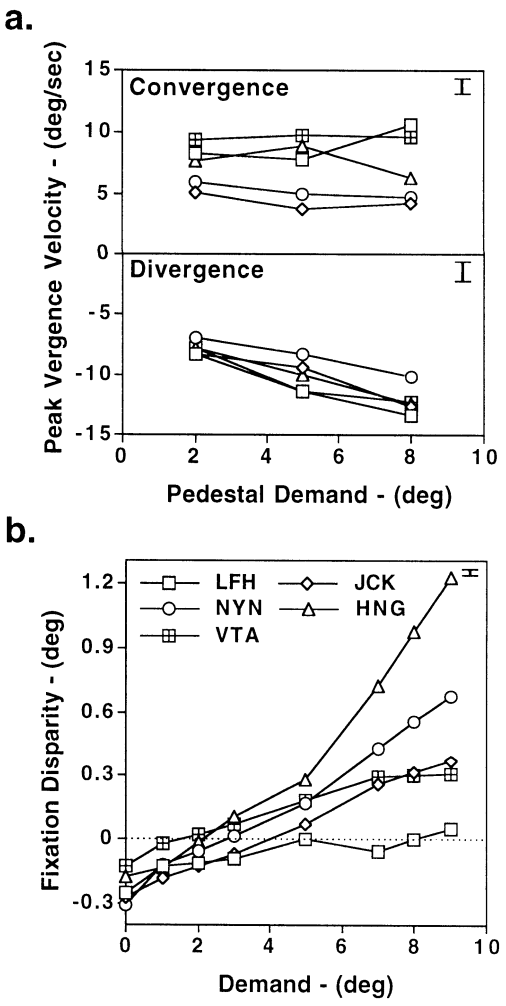

are opposite to the predictions of the open-loop relationship between disparity and vergence velocity (Rashbass & Westheimer, 1961), which suggests that the magnitude of vergence velocity should increase with increases in stimulating step size. This indicates that the effect of pedestal demand on vergence velocity cannot be explained by the corresponding changes in fixation disparity. Our analysis also indicates that pedestal vergence demand does not affect the time at which peak convergence velocity and peak divergence velocity occur, thus ruling out the possibility of pedestal demand-dependent changes in reaction time within the vergence system.

4.3 Is Fixation Disparity Due to Asymmetry in Vergence Dynamics? We tested the quantitative relationship between $E(V)$ and $\lambda(V)$ as predicted by the static vergence model. Due to the small-signal linearity exhibited by the vergence system around a given pedestal demand (Rashbass & Westheimer, 1961), $\gamma(V)$ during a small vergence step response ($\sim \pm 2$ degrees) is approximated by:

$$\gamma(V) \approx \sqrt{\frac{\text{Peak convergence velocity around V / Corrected convergence step input}}{\text{Peak divergence velocity around V / Correctred divergence step input}}}. \tag{4.1}$$

Figure 7b shows the computed sensory motor gains for convergence and divergence pathways. A three-way repeated measures ANOVA indicates a significant difference between convergence and divergence gains ($F[1, 4] = 11.9$, $p = .03$). The magnitude of average divergence gain increases with an increase in pedestal demand, while the convergence gain decreases slightly, as expected for subjects who exhibit underconvergence.

To determine the relationship between fixation disparity and vergence asymmetry, $\gamma(V)$ was computed from the data shown in Figures 6a and 7a using equation 4.1. $\lambda(V)$ was computed from $\gamma(V)$ using equation 2.16. Standard error propagation techniques (Bevington, 1969) were used to transform standard error estimates in all calculations. Figure 8a shows the linear relationship between $\lambda(V)$ and fixation disparity $E(V)$ for all subjects.

Figure 6: *Facing page.* Peak convergence and divergence velocities and fixation disparities. The symbols for subjects are same in all subsequent figures and are shown in *b*. (a) Average peak convergence and divergence velocities and their relationship with the pedestal convergence demand for five subjects. The maximum standard error (the bar shown in the upper left column of each panel) in velocity for any subject was 0.96 degree per second for convergence velocity and 1.37 degrees per second for divergence velocity. The number of observations ranged from two to six. (b) Average fixation disparities for various step demands within a staircase paradigm. Positive values on the *y*-axis indicate underconvergence. The largest staircase, which consisted of a 1 degree first step, followed by four consecutive 2 degree steps, is generated when using an 8 degree pedestal demand. Note that the 8 degree pedestal demand is obtained by toggling the three pulses between 7 and 9 degree demands. The fixation disparity values for 2 and 8 degree demands are interpolated by averaging the fixation disparities from corresponding neighboring demands. For example, the fixation disparity for 2 degree demand is the average of fixation disparities at 1 and 3 degree demands. The maximum standard error (bar shown in upper left column) in fixation disparity for any subject was 0.024 degree. The number of observations ranged from two to six.

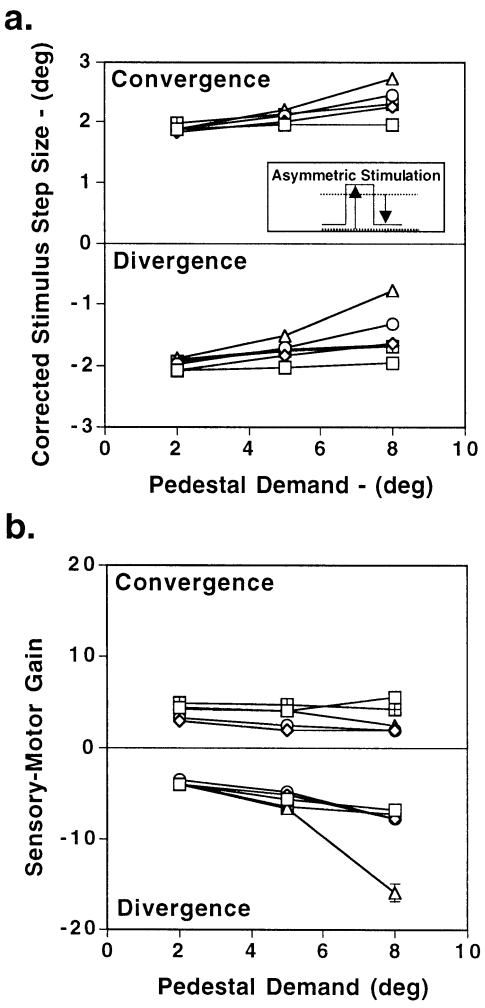

Notice also that the gains for convergence and divergence are very similar for the lowest pedestal demand (see Figure 7b). As shown in Figure 8a, the fixation disparity for four out of five subjects is very close to zero at the lowest demand, thus supporting the prediction of the static vergence model that relates zero error to perfect symmetry ($\lambda(V) = 0$). The fifth subject (*JCK*) shows a small bias that may be due to a constant physiological or anatomical error with respect to the optical axis. Figure 8a also shows the nature of intersubject as being primarily noninteracting. Hence, our results strongly suggest that fixation disparity arises from an asymmetry between the dynamics of convergence and divergence pathways when stimulated

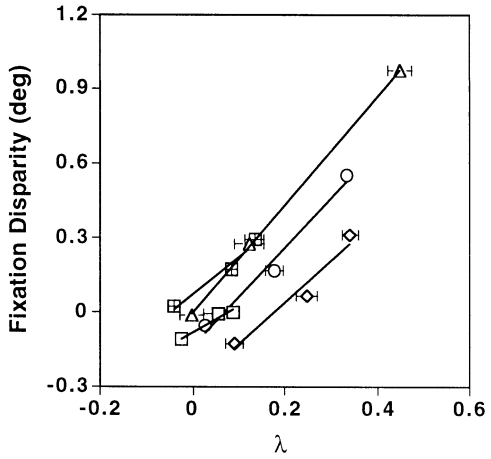

Figure 8: Relationship between fixation disparity $E(V)$ and $\lambda(V)$ for five subjects. Positive fixation disparity indicates underconvergence. Least-square linear regression lines are fit for each subject using data from three pedestal demands.

by a disparity spread. An exceptional feature of our explanation is that it does not require a leaky position integrator in the vergence system, illustrating that steady-state errors can arise in nonleaky negative feedback neural control systems.

4.4 Fixation Disparity and Closed-Loop Accommodation. Most clinical fixation disparity measurements are obtained under a closed-loop accommodation condition (Ogle et al., 1967); therefore, it is necessary to comment on the influence of accommodation upon fixation disparity and how it relates to the model presented here. It has been previously shown that

Figure 7: *Facing page.* Asymmetric stimulation and sensory motor gains. (a) The stimulating step sizes at various pedestal demands after correcting for corresponding fixation disparities. Recall that the uncorrected step size is 2 degrees for convergence and divergence movements. The inset illustrates the asymmetric stimulation induced by a symmetric external stimulus (demand) in the presence of fixation disparity. The dotted line is the vergence angle for the corresponding demand shown in solid lines (pulse). The difference between the solid and dotted lines is the fixation disparity. The up (down) arrow indicates the actual convergence (divergence) step input to the vergence system. (b) Average sensory motor gains of convergence and divergence pathways as a function of pedestal demand for five subjects. The convergence (divergence) gains are computed using the numerator (denominator) under the square-root sign of equation 4.1. The error bars in all figures represent ± 1 standard error.

the slope of the relationship between fixation disparity and vergence demand is modified when accommodation operates in open- versus closed-loop condition. Semmlow and Hung (1979) have shown that the slope of fixation disparity curve becomes *shallower* when accommodation operates in open-loop compared to closed-loop condition, and their data are consistent with current models of accommodation and vergence (Hung & Semmlow, 1980; Schor, 1992). Contrary to Semmlow and Hung's data, Hessler, Pickwell, and Gilchrist (1989) have shown that the slope of fixation disparity curve becomes *steeper* when accommodation operates in open-loop compared to closed-loop condition. Regardless of the actual sign of the change in slope, one can determine the fixation disparity curve under a closed-loop accommodation condition from that under the open-loop accommodation condition by adding a term,

$$FD(V, A) = E(V) + \alpha V + \beta A + \delta, \tag{4.2}$$

where α represents the change in slope of the fixation disparity curve from the closed-loop to open-loop accommodation condition, β represents the shift in fixation disparity curve due to accommodation, δ is a constant bias, and A is the accommodative demand. Note that the above analysis is approximate, and it assumes linear interactions between the accommodation and the vergence systems, as suggested by current models of accommodation and vergence (Hung & Semmlow, 1980; Schor, 1992). Ogle et al. (1967) showed that for many subjects, the fixation disparity curves did not merely shift but also changed shapes when accommodation changed from far to near and vice versa. This phenomenon cannot be explained by linear interactions of vergence and accommodation and points to a severe limitation of existing models of accommodation and vergence. Further, Wick and Joubert (1988) have shown that blur affects fixation disparity in a highly nonlinear way. A more formal and accurate analysis based on our model requires a complete neural network model of accommodation and vergence.

5 Other Factors Affecting Fixation Disparity

Several vergence parameters other than those considered in our model are also shown to influence fixation disparity. Vergence adaptation, resulting from prolonged binocular viewing, is known to reduce fixation disparity (Schor 1979a, 1979b; Carter, 1980; Schor, 1980). After vergence adaptation, the fixation disparity at certain demands has been shown to be correlated with the decay of vergence in darkness (Schor et al., 1986). Proximal cues also influence the magnitude of fixation disparity (North, Henson, & Smith, 1993). Viewing distance in some cases alters the form of fixation disparity in the same subjects (Ogle et al., 1967; Kruza, 1993). Contrary to the results of Palmer and von Noorden (1978), heterophorias measured at near distances are shown to be correlated with fixation disparity (Schor, 1983). Dark

vergence is also known to have correlation with fixation disparity (Kruza, 1994). However, since fixation disparity is observed under conditions that eliminate (or keep fixed) the aforementioned parameters (i.e., in the absence of adaptation, for stimuli without proximal cues, when accommodation input and viewing distance are kept constant), we suggest that these are *modulatory effects*, rather than being the basic neural origin of fixation disparity. These factors may affect fixation disparity indirectly via changes in vergence dynamics. Future work can assess the relative contribution of these modulatory factors in determining vergence dynamics and fixation disparity.

Summary

As opposed to an explanation of fixation disparity based on control-type models of the vergence system, our explanation is based on a model that has neurophysiological correlates in primates and has successfully explained most of vergence dynamic data. Our experiments and analysis show that fixation disparity can arise due to the asymmetry in the dynamics of the convergence and divergence pathways when stimulated by a distributed disparity code. Further, our explanation remains consistent with the non-leaky position integration property of the vergence system; we show that neural leakage is not necessary to explain steady-state errors in the vergence system and presumably in other sensorimotor systems driven by distributed sensory coding.

Appendix

We have used the same equations (and terminology) that were presented in earlier work describing the neural network model of the vergence system (Patel et. al., 1997) to show the relationship between the experimental findings of Rashbass and Westheimer (1961) and the functions describing the transformation from the output of disparity encoders to the output of velocity cells in the model. A convention used in this appendix is that the equations with capital letters belong to the previous article (Patel et. al., 1997) and those with lowercase letters are described in this article. We consider the situation in which the input (or disparity) is clamped (fixed) in time and the output (vergence angle) is temporally changing.

Since the input signal is fixed in time, we can consider the disparity encoders to be in a steady state. The activity of the disparity encoders (eq A.5 in the previous article) will be represented by a temporally fixed and spatially distributed activity. For simplicity, we chose a binary rectangular spread. Thus:

$$f_{DC}(x_{DC,d}) = \begin{Bmatrix} 1 & \text{if } d_s - \frac{n}{2} \le d \le d_s + \frac{n}{2} \\ 0 & \text{otherwise} \end{Bmatrix}, \tag{a.1}$$

where d is the index of the disparity encoder cell representing disparity d, d_s is the average stimulus disparity, and n is the total spread of activity across disparity encoder cells.

The output of the disparity encoder cells feeds into the convergence and divergence velocity cells via the positive synaptic weights $w_{d,v\Uparrow}$ and $w_{d,v\Downarrow}$. The dynamics of the velocity cells is governed by equations A.6 and A.7, which are rewritten below:

$$K_s \frac{dx_{v\Uparrow}}{dt} = -A_{v\Uparrow} x_{v\Uparrow} + \sum_{2N}^{d=0} w_{d,v\Uparrow} f_{DC}(x_{DC}, d) \tag{a.2}$$

$$K_s \frac{dx_{v\Downarrow}}{dt} = -A_{v\Downarrow} x_{v\Downarrow} + \sum_{d=-2N}^{0} w_{d,v\Downarrow} f_{DC}(x_{DC}, d), \tag{a.3}$$

where $x_{v\Uparrow}(x_{v\Downarrow})$ is the activity of the convergence (divergence) velocity cell, $A_{v\Uparrow}(A_{v\Downarrow})$ is the decay constant of the convergence (divergence) velocity cell, $-2N \le d \le 2N$, f_{DC} is the firing-rate function of the disparity encoder cells (same form as equation A.1; also see equation a.13), and K_s is a scaling constant.

The position cells integrate the outputs of the velocity cells according to the following shunting push-pull equations (same as equation A.8):

$$K_s \frac{dx_{p\Uparrow}}{dt} = \left(B_{p\Uparrow} - x_{p\Uparrow}\right) w_{v\Uparrow,p\Uparrow} f_{v\Uparrow}(x_{v\Uparrow}) - (D_{p\Uparrow} + x_{p\Uparrow}) w_{v\Downarrow,p\Uparrow} f_{v\Downarrow}(x_{v\Downarrow}) \tag{a.4}$$

$$K_s \frac{dx_{p\Downarrow}}{dt} = \left(B_{p\Downarrow} - x_{p\Downarrow}\right) w_{v\Downarrow,p\Downarrow} f_{v\Downarrow}(x_{v\Downarrow}) - (D_{p\Downarrow} + x_{p\Downarrow}) w_{v\Uparrow,p\Downarrow} f_{v\Uparrow}(x_{v\Uparrow}), \tag{a.5}$$

where, $x_{p\Uparrow}(x_{p\Downarrow})$ is the activity of the convergence (divergence) position cell, $B_{p\Uparrow}(B_{p\Downarrow})$ is the upper bound for the activity of convergence (divergence) position cell, $w_{v\Uparrow,p\Uparrow}(w_{v\Uparrow,p\Downarrow})$ and $w_{v\Downarrow,p\Uparrow}(w_{v\Downarrow,p\Downarrow})$ are the synaptic weights between the output of the convergence and divergence velocity cells and the input to the convergence (divergence) position cells respectively, $f_{v\Uparrow}(f_{v\Downarrow})$ is the firing-rate function of the convergence (divergence) velocity cell, and $-D_{p\Uparrow}(-D_{p\Downarrow})$ is the lower bound for the activity of convergence (divergence) position cell. Notice the absence of the passive decay term due to which the integration by the position cells is nonleaky.

Finally, the output of the position cells drives the motoneurons and the plant of the left and the right eye whose dynamics are described by the following equations (same as equation A.17 but without the last two terms):

$$K_p \frac{d\theta^L}{dt} = -\frac{1}{\tau^L}\theta^L + K^L_{p\Uparrow} f_{p\Uparrow}(x_{p\Uparrow}) - K^L_{p\Downarrow} f_{p\Downarrow}(x_{p\Downarrow}) \tag{a.6}$$

$$K_p \frac{d\theta^R}{dt} = -\frac{1}{\tau}\theta^R + K^R_{p\Downarrow} f_{p\Downarrow}(x_{p\Downarrow}) - K^R_{p\Uparrow} f_{p\Downarrow}(x_{p\Uparrow}), \tag{a.7}$$

where $\theta^L(\theta^R)$ is the position of the left (eye) eye in the head, $\tau^L(\tau^R)$ is the time constant of the motoneuron and the plant system of the left (right) eye, $K^L_{p\Uparrow}(K^R_{p\Uparrow})$ and $K^L_{p\Downarrow}(K^R_{p\Downarrow})$ are the gain of the convergence and divergence position cells for the left (right) eye, $f_{p\Uparrow}(f_{p\Downarrow})$ is the firing rate function of the convergence (divergence) position cell, and K_p is a scaling constant. For simplicity, we have ignored the signals from the velocity overdrive circuit.

Now let us consider Rashbass and Westheimer's (1961) experiment. In this experiment, the input (or disparity) was clamped (help constant) and the vergence velocity was measured. The finding is that within a small range of disparities (at least ± 2 degrees, see Figure 22 in Rashbass and Westheimer, 1961), the eye velocity (which remained almost constant in time) is a linear function of the clamped disparity. Let us apply this finding to our model. The dependent variable in the experiment is the vergence velocity (V_{rw}) and is defined by

$$\frac{dV_{rw}}{dt} = \frac{d}{dt}(\theta^L - \theta^R). \tag{a.8}$$

The finding is that

$$\frac{dV_{rw}}{dt} = K_{rw} d_s, \tag{a.9}$$

where K_{rw} is a constant estimated to be about 10 degrees per second per degree of disparity and d_s is the average target disparity. By substituting equations a.6 and a.7 in equation a.8, we have

$$K_{rw} d_s = \frac{1}{K_p}\left\{-\frac{1}{\tau^L}\theta^L + \frac{1}{\tau^R}\theta^R + \left(K^L_{p\Uparrow} + K^R_{p\Uparrow}\right) f_{p\Uparrow}(x_{p\Uparrow}) - \left(K^L_{p\Downarrow} + K^R_{p\Downarrow}\right) f_{p\Downarrow}(x_{p\Downarrow})\right\}.$$

By using $K^L_{p\Uparrow} + K^R_{p\Uparrow} = \Delta_{p\Uparrow}$, $K^L_{p\Downarrow} + K^R_{p\Downarrow} = \Delta_{p\Downarrow}$ and $\tau^L = \tau^R = \tau$ in the previous equation, we have

$$K_{rw} d_s = \frac{1}{K_p}\left\{-\frac{1}{\tau}(\theta^L - \theta^R) + \Delta_{p\Uparrow} f_{p\Uparrow}(x_{p\Uparrow}) - \Delta_{p\Downarrow} f_{p\Downarrow}(x_{p\Downarrow})\right\}. \tag{a.10}$$

Differentiating both sides of equation a.10 and using Rashbass and Westheimer's results from equation a.9 give:

$$0 = -\frac{1}{\tau} K_{rw} d_s + \Delta_{p\Uparrow} f'_{p\Uparrow}(x_{p\Uparrow})\dot{x}_{p\Uparrow} - \Delta_{p\Downarrow} f'_{p\Downarrow}(x_{p\Downarrow})\dot{x}_{p\Downarrow} \tag{a.11}$$

Because, the target used in Rashbass and Westheimer's experiments was very small (0.08 degree wide), the results obtained in their experiments

are likely due to the case where $d_s \geq \frac{n}{2}$. In this case, the disparity spread remains on either the convergence or the divergence side, and only one of the two sensory pathways is activated. For definiteness, assume only the convergence pathway is activated. Starting from equation a.11, we have:

$$\frac{1}{\tau}K_{rw}d_s = \Delta_{p\Uparrow} f'_{p\Uparrow}(x_{p\Uparrow}) - \Delta_{p\Downarrow} f'_{p\Downarrow}(x_{p\Downarrow})\dot{x}_{p\Downarrow}. \tag{a.12}$$

The function $f'_{p\Uparrow}$ was chosen to have the form as (same as equation A.1):

$$f(x) = \begin{Bmatrix} 0 & \text{if } x, \Gamma \\ \alpha x & \text{if } \Gamma \leq x\Omega \\ \alpha\Omega & \text{if } \leq x \end{Bmatrix}, \tag{a.13}$$

where Γ, Ω, and α are constants determining the threshold, saturation, and gain of the firing function respectively.

Because the position cells are active, $x_{p\Uparrow} > \Gamma$ and $x_{p\Downarrow} > \Gamma$, and because the experiment is conducted for small disparities and measurements are made before the eye plant system saturates, we have $\Gamma \leq x_{p\Uparrow} \leq \Omega$ and $\Gamma \leq x_{p\Downarrow} \leq \Omega$, $f_{p\Uparrow}(x_{p\Uparrow}) = \alpha_{p\Uparrow} x_{p\Uparrow}$ and $f_{p\Downarrow}(x_{p\Downarrow}) = \alpha_{p\Downarrow} x_{p\Downarrow}$, and $f'_{p\Uparrow}(x_{p\Uparrow}) = \alpha_{p\Uparrow}$ and $f'_{p\Downarrow}(x_{p\Downarrow}) = \alpha_{p\Downarrow}$. Further, if we assume that the convergence and divergence position cells have identical parameters (see Table B1 in Patel et al., 1997) and the plant characteristics are identical downstream from the position cells for convergence and divergence (see Table 3 in Patel et al., 1997), then $\alpha_{p\Uparrow} = \alpha_{p\Downarrow} = \alpha_p$ and $\Delta_{p\Uparrow} = \Delta_{p\Downarrow} = \Delta$. Therefore equation a.12 becomes

$$\frac{1}{\tau}K_{rw}d_s = \Delta\alpha_p \left\{\dot{x}_{p\Uparrow} - \dot{x}_{p\Downarrow}\right\}. \tag{a.14}$$

By substituting equations a.4 and a.5 in equation a.14, we have

$$\begin{aligned} \frac{K_s K_{rw} d_s}{\tau \Delta_{p\Uparrow}\alpha_{p\Uparrow}} = {} & (B_{p\Uparrow} - x_{p\Uparrow}) w_{v\Uparrow,p\Uparrow} f_{v\Uparrow}(x_{v\Uparrow}) - (D_{p\Uparrow} + x_{p\Uparrow}) w_{v\Downarrow,p\Uparrow} f_{v\Downarrow}(x_{v\Downarrow}) \\ & - (B_{p\Downarrow} - x_{p\Downarrow}) w_{v\Downarrow,p\Downarrow} f_{v\Downarrow}(x_{v\Downarrow}) \\ & + (D_{p\Downarrow} + x_{p\Downarrow}) w_{v\Uparrow,p\Downarrow} f_{v\Uparrow}(x_{v\Uparrow}). \end{aligned} \tag{a.15}$$

Because only convergence sensory pathway is active, $f_{v\Downarrow}(x_{v\Downarrow}) = 0$. Also, as mentioned earlier, because the data in Rashbass and Westheimer's study were collected for a small range of eye positions (from initial convergence of 1.7 degrees) or only the initial portion (within the delay period) of the vergence eye movement, we have $x_{p\Uparrow} << B_{p\Uparrow}$ and $x_{p\Downarrow} << B_{p\Downarrow}$. In addition, because the velocity cell was above threshold and not saturated, $f_{v\Uparrow}(x_{v\Uparrow}) = \alpha_{v\Uparrow} x_{v\Uparrow}$. Further, because the convergence and divergence position cells are assumed to have the same parameters, $B_{p\Uparrow} = B_{p\Downarrow} = B$ and $D_{p\Uparrow} = D_{p\Downarrow} = D$. In our dynamic model, the upper and the lower limits of activation for the

position cells are symmetric around 0, thus, (see Table B1 in Patel et al., 1997). The push-pull connectivity between the position cells and the velocity cells is also symmetric; thus, $w_{v\Uparrow,p\Uparrow} = w_{v\Uparrow,p\Downarrow} = w_{v\Downarrow,p\Uparrow} = w_{v\Downarrow,p\Downarrow} = w_{v,p}$. Note that $w_{v\Uparrow,p\Downarrow}$ and $w_{v\Downarrow,p\Uparrow}$ in Table 2 in Patel et al., 1997 have a negative sign. The sign indicates only the inhibitory nature of the synapses, and for the purpose of using it with the equations A.8 and A.16 and a.15, only the magnitude should be used. The signs for $w_{v\Uparrow,p\Downarrow}$ and $w_{v\Downarrow,p\Uparrow}$ were inadvertently left in Table 2 in Patel et al., 1997. Therefore, equation a.15 can be rewritten as

$$\frac{K_s K_{rw} d_s}{\tau \Delta\alpha_p} = 2B w_{v,p} \alpha_{v\Uparrow} x_{v\Uparrow}, \tag{a.16}$$

which yields

$$x_{v\Uparrow} = \frac{K_s K_{rw} d_s}{2\tau \Delta\alpha_p B w_{v,p} \alpha_v}. \tag{a.17}$$

Consider now the equations for the velocity cells. Because during Rashbass and Westheimer's experiments, disparity was held constant and because the time constant of the velocity cell is much shorter than the circuits following it (position integration and plant), the velocity cell can be considered to be in steady state. By letting $\dot{x}_{v\Uparrow} = 0$ in equation a.2, we obtain

$$x_{v\Uparrow} = \frac{1}{A_{v\Uparrow}} \sum_{0}^{2N} w_{d,v\Uparrow} f_{DC}(x_{DC,d}). \tag{a.18}$$

To simply our analysis and given the dense packing of disparity encoder cells, instead of using the discrete index d for disparity, we will use a continuous variable z. Positive (negative) values of z represent convergence (divergence) disparities. Equation a.18 becomes

$$x_{v\Uparrow} = \frac{1}{A_{v\Uparrow}} \int_{0}^{2N} w_{v\Uparrow}(z) f_{DC}(x_{DC}(z)) dz. \tag{a.19}$$

Now, given that the disparity is encoded by a binary rectangular distribution (see equation a.1), we obtain

$$x_{v\Uparrow} = \frac{1}{A_{v\Uparrow}} \int_{d_s - \frac{n}{2}}^{d_s + \frac{n}{2}} w_{v\Uparrow}(z) dz. \tag{a.20}$$

By combining equations A.17 and A.20 we get

$$C d_s = \int_{d_s - \frac{n}{2}}^{d_s + \frac{n}{2}} w_{v\Uparrow}(z) dz, \tag{a.21}$$

where

$$C = \frac{K_s K_{rw} A_{v\Uparrow}}{2\tau \Delta\alpha_p B w_{v,p} \alpha_v} \tag{a.22}$$

Equation A.21 holds for $|d_s| \leq\sim 2$ degrees. From this equation, we can write

$$w_{v\Uparrow}(z) = \frac{C}{n} z. \tag{a.23}$$

Thus, we show that Rashbass and Westheimer's result implies a linear relationship between the weights from the disparity encoders to the velocity cells and disparity. Note that the relationship described in equation a.23 is obtained for $d_s \geq \frac{n}{2}$ and is assumed to hold for $0 < d_s < \frac{n}{2}$.

Acknowledgments

We thank Harold Bedell for his invaluable comments and suggestions on this article. We also thank the reviewers for helping us improve this manuscript substantially. This work was supported by NIH grants EY08862, MH49892, and EY07551 and a postdoctoral fellowship from ISSO of University of Houston.

References

Barlow, H. B., Blakemore, C., & Pettigrew, J. D. (1967). The neural mechanism of binocular depth discrimination. *Journal of Physiology, 193*, 327–342.

Bevington, P. R. (1969), *Data reduction and error analysis for the physical sciences*, New York: McGraw-Hill.

Campbell, F. W. (1954). The minimum quantity of light required to elicit the accommodation reflex in man. *Journal of Physiology, 123*, 357–366.

Carter, D. B. (1980). Parameters of fixation disparity. *American Journal of Optometry and Physiological Optics, 57*, 610–617.

Charman, W. N. (1991). Optics of the human eye. In W. N. Charman (Ed.), *Visual optics and instrumentation, Vol. 1. Vision and visual dysfunction*. New York: Macmillan.

Crane, H. D., & Steele, C. M. (1978). Accurate three-dimensional eyetracker. *Applied Optics, 17*, 691–705.

Cumming, B. G., & Parker A. J. (1997). Responses of primary visual cortical neurons to binocular disparity without depth perception. *Nature, 389*, 280–283.

Enright, J. T. (1986). Facilitation of vergence changes by saccades: Influences of misfocused images and of disparity stimuli in man. *Journal of Physiology, 371*, 69–87.

Erkelens, C. J., Steinman, R. M., & Collewijn H. (1989). Ocular vergence under natural conditions I. Continuous changes of target distance along the median plane. *Proceedings of the Royal Society, London, 236*, 417–440.

Gamlin, P. D., Gnadt, J. W., & Mays, L. E. (1989). Abducen internuclear neurons carry an inappropriate signal for ocular convergence. *Journal of Neurophysiology, 62*, 70–81.

Gamlin, P. D., & Mays, L. E. (1992). Dynamic properties of medial rectus motoneurons during vergence eye movements. *Journal of Neurophysiology, 67*, 64–74.

Gonzalez, F., Relova, J. L., Perez, R., Acuna, C., & Alonso, J. M. (1993). Cell responses to vertical and horizontal retinal disparities in the monkey visual cortex. *Neuroscience Letter, 160*, 167–170.

Grossberg, S. (1988). Nonlinear neural networks: Principles, mechanisms, and architectures. *Neural Networks, 1*, 17–61.

Hessler, J., Pickwell, D., & Gilchrist, J. (1989). The accommodative contribution to binocular vergence eye movements. *Ophthalmic Physiological Optics, 9*, 379–384.

Hung, G. K., & Semmlow, J. L. (1980). Static behavior of accommodation and vergence: Computer simulation of an interactive dual-feedback system. *IEEE Transactions on Biomedical Engineering, 27*, 439–447.

Hung, G. K, Zhu, H. M., & Ciuffreda, K. J. (1997). Convergence and divergence exhibit different response characteristics to symmetric stimuli. *Vision Research, 37*, 1197–1205.

Johnson, C. A. (1976). Effects of luminance and stimulus distance on accommodation and visual resolution. *Journal of the Optical Society of America, 66*, 138–142.

Keller, E. L. (1981), *In models of oculomotor behavior and control*. Florida: CRC Press.

Krishnan, V. V. & Stark, L. (1977). A heuristic model for human vergence eye movement system. *IEEE Transactions on Biomedical Engineering, 24*, 44–49.

Krishnan, V. V., & Stark, L. (1983). *Vergence eye movements: Basic and clinical aspects*. Boston: Butterworths.

Kruza, W. J. (1993). Fixation disparity at different viewing distances of a visual display unit. *Ophthalmic Physiological Optics, 13*, 27–34.

Kruza, W. J. (1994). Dark vergence in relation to fixation disparity at different luminance and blur levels. *Vision Research, 34*, 1197–1204.

Mallot, H. A., Roll, A., & Arndt P. A. (1996). Disparity-evoked vergence is driven by interocular correlation. *Vision Research, 36*, 2925–2837.

Masson, G. S., Busettini, C., & Miles F. A. (1997). Vergence eye movements in response to binocular disparity without depth perception. *Nature, 389*, 283–286.

Mays, L. E. (1984). Neural control of eye movements: Convergence and divergence neurons in midbrain. *Journal of Neurophysiology, 51*, 1091–1108.

Mays, L. E., Porter, J. D., Gamlin, P. D. R., & Tello, C. A. (1986). Neural control of vergence eye movements: Neurons encoding vergence velocity. *Journal of Neurophysiology, 56*, 1007–1021.

North, R. V., Henson, D. B., & Smith, T. J. (1993). Influence of proximal, accommodative and disparity stimuli upon the vergence system. *Ophthalmic Physiological Optics, 13*, 239–243.

Ogle, K. N., Martens, T. G., & Dyer, J. A. (1967). *Oculomotor imbalance in binocular vision and fixation disparity*. Philadelphia: Lea Febiger.

Palmer, E. A., & von Noorden, G. K. (1978). The relationship between fixation disparity and heterophoria. *American Journal of Ophthalmology, 86*, 172–176.

Patel, S. S., Ogmen, H., & Jiang, B. (1996). Steady-state vergence errors modeled by asymmetry in convergence and divergence sub-systems. *Investigative Ophthalmology and Visual Science, 37*, S164.

Patel, S. S., Ogmen, H., White, J. M., & Jiang, B. (1997). Neural network model of short term disparity vergence dynamics. *Vision Research, 37*, 1383–1400.

Pobuda, M., & Erkelens, C. J. (1993). The relationship between absolute disparity and ocular vergence. *Biological Cybernetics, 68*, 221–228.

Poggio, G. F., Gonzalez F., & Krause, F. (1988). The relationship between absolute disparity and ocular vergence. *Journal of Neuroscience, 8*, 4531–4550.

Rashbass, C., & Westheimer G. (1961). Disjunctive eye movements. *Journal of Physiology, 159*, 339–360.

Robinson, D. A. (1981). The use of control system analysis in neurophysiology of eye movements. *Annual Reviews of Neuroscience, 4*, 463–503.

Roy J. P, Komatsu H., & Wurtz R. H. (1992). Disparity sensitivity of neurons in monkey extrastriate area MST. *Journal of Neuroscience, 12*, 2478–2492.

Saladin, J. J. (1986). Convergence insufficiency, fixation disparity, and control system analysis. *American Journal of Optometry & Physiological Optics, 63*, 645–653.

Schor, C. M. (1979a). The influence of rapid prism adaptation upon fixation disparity. *Vision Research, 19*, 757–765.

Schor, C. M. (1979b). The relationship between fusional vergence eye movements and fixation disparity. *Vision Research, 19*, 1359–1367.

Schor, C. M. (1980). Fixation of disparity: A steady state error of disparity-induced vergence. *American Journal of Optometry and Physiological Optics, 57*, 618–631.

Schor, C. M. (1983). Fixation disparity and vergence adaptation. In C. M. Schor, & K. J. Ciuffreda (Eds.), *Vergence eye movements: Basic and clinical aspects* (pp. 465–516). Boston, Butterworth-Heinemann.

Schor, C. M. (1992). A dynamic model of cross-coupling between accommodation and convergence: Simulations of step and frequency responses. *Optometry and Vision Science, 69*, 258–269.

Schor, C. M., Robertson, K. M., & Wesson, M. (1986). Disparity vergence dynamics and fixation disparity. *American Journal of Optometry and Physiological Optics, 63*, 611–618.

Semmlow, J. L., & Hung, G. K. (1979). Accommodative and fusional components of fixation disparity. *Investigative Ophthalmology Visual Science, 18*, 1082–1086.

Semmlow, J. L., Hung, G. K., Horng, J. L., & Ciuffreda, K. J. (1994). Disparity vergence eye movements exhibit preprogrammed motor control. *Vision Research, 34*, 1335–1343.

Sethi, B. (1986). Vergence adaptation: A review. *Documenta Ophthalmologica, 63*, 247–263.

Stevenson, S. B., Cormack, L. K., & Schor, C. M. (1994). The effect of stimulus contrast and interocular correlation on disparity vergence. *Vision Research, 34*, 383–396

Wagner, H., & Frost, B. (1993) Disparity sensitive cells in the owl have a characteristic disparity. *Nature, 364*, 796–798.

Wick, B., & Bedell, H. E (1992). Rapid- and slow-velocity vergence eye movements. *Ophthalmic Physiological Optics, 12*, 420–424.

Wick, B., & Joubert, C. (1988). Lens-induced fixation disparity curves. *American Journal of Optometry and Physiological Optics, 65*, 606–612.

Yang, D. S., Fitzgibbon, E. J., & Miles F. A. (1998). Short-latency vergence eye movements induced by radial optic flow in humans: Dependence on the preexisting vergence state. *Society for Neuroscience Abstract, 24*, 1889.

Zee, D. S., Fitzgibbon, E. J., & Optican, L. M. (1992). Saccade-vergence interactions in humans. *Journal of Neurophysiology, 68*, 1624–1641.

Zuber, B. L., & Stark, L. (1968). Dynamical characteristics of the fusional vergence eye-movement system. *IEEE Transactions on Systems Science and Cybernetics, 4*, 72–79.

Received September 21, 1998; accepted September 12, 2000.